JCI The Journal of Clinical Investigation

Keratinocyte-derived microvesicle particles mediate ultraviolet B radiation–induced systemic immunosuppression

Langni Liu, … , R. Michael Johnson, Jeffrey B. Travers

J Clin Invest. 2021;131(10):e144963. https://doi.org/10.1172/JCI144963.

Research Article | Dermatology | Immunology

Graphical abstract

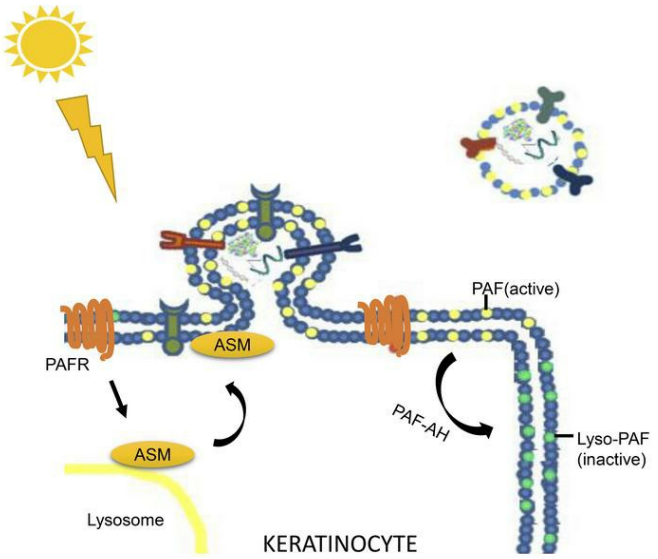

Keratinocyte-derived microvesicle particles mediate ultraviolet B radiation–induced systemic immunosuppression

Langni Liu,[1] Azeezat A. Awoyemi,[1] Katherine E. Fahy,[1] Pariksha Thapa,[1] Christina Borchers,[1] Benita Y. Wu,[1] Cameron L. McGlone,[1] Benjamin Schmeusser,[1] Zafer Sattouf,[1] Craig A. Rohan,[1,2] Amy R. Williams,[1] Elizabeth E. Cates,[1] Christina Knisely,[1] Lisa E. Kelly,[1] Ji C. Bihl,[1] David R. Cool,[1] Ravi P. Sahu,[1] Jinju Wang,[1] Yanfang Chen,[1] Christine M. Rapp,[1] Michael G. Kemp,[1] R. Michael Johnson,[3] and Jeffrey B. Travers[1,2,4]

[1]Department of Pharmacology and Toxicology, [2]Department of Dermatology, and [3]Department of Plastic Surgery, Wright State University, Dayton, Ohio, USA. [4]Dayton VA Medical Center, Dayton, Ohio, USA.

A complete carcinogen, ultraviolet B (UVB) radiation (290–320 nm), is the major cause of skin cancer. UVB-induced systemic immunosuppression that contributes to photocarcinogenesis is due to the glycerophosphocholine-derived lipid mediator platelet-activating factor (PAF). A major question in photobiology is how UVB radiation, which only absorbs appreciably in the epidermal layers of skin, can generate systemic effects. UVB exposure and PAF receptor (PAFR) activation in keratinocytes induce the release of large numbers of microvesicle particles (MVPs; extracellular vesicles ranging from 100 to 1000 nm in size). MVPs released from skin keratinocytes in vitro in response to UVB (UVB-MVPs) are dependent on the keratinocyte PAFR. Here, we used both pharmacologic and genetic approaches in cells and mice to show that both the PAFR and enzyme acid sphingomyelinase (aSMase) were necessary for UVB-MVP generation. Our discovery that the calcium-sensing receptor is a keratinocyte-selective MVP marker allowed us to determine that UVB-MVPs leaving the keratinocyte can be found systemically in mice and humans following UVB exposure. Moreover, we found that UVB-MVPs contained bioactive contents including PAFR agonists that allowed them to serve as effectors for UVB downstream effects, in particular UVB-mediated systemic immunosuppression.

Introduction

Ultraviolet B (UVB) radiation (290–320 nm) is both a mutagen and an immunosuppressant and is a primary cause of skin cancer (1, 2). UVB-induced systemic immunosuppression is due to the glycerophosphocholine-derived lipid mediator platelet-activating factor (PAF) in a process involving cyclooxygenase-2–derived prostaglandins and histamine/chemokine-regulated cell chemotaxis that promotes mast cell migration to draining lymph nodes, where they activate Tregs and potentially regulatory B cells and thereby contribute to photocarcinogenesis (3–7). Although this UVB-mediated systemic immunosuppressive pathway has been characterized, a major question that remains is how metabolically labile PAF agonists leave the epidermis.

Formed in response to diverse stressors, subcellular microvesicle particles (MVPs), which form from the plasma membrane, have been demonstrated to transport various bioactive substances (8, 9). Recent studies have implicated MVPs as potential effectors for UVB. In particular, UVB irradiation of the keratinocyte-derived human cell line HaCaT as well as human skin explants results in PAF receptor (PAFR) signaling–dependent MVP release (10, 11).

Conflict of interest: The authors have declared that no conflict of interest exists.

Submitted: October 7, 2020; **Accepted:** April 7, 2021; **Published:** April 8, 2021.
Reference information: *J Clin Invest*. 2021;131(10):e144963.
https://doi.org/10.1172/JCI144963.

Although increased MVPs have been described in inflammatory disorders such as lupus erythematosus and psoriasis, the source of MVPs and overall pathologic significance are as yet unclear (12, 13). The present studies sought to define the metabolic pathway by which MVPs are generated by keratinocytes in response to UVB (UVB-MVPs) and their significance in UVB-mediated effects. We also report here that MVPs derived from keratinocytes express the calcium-sensing receptor (CaSR) (14, 15), which allowed us to test complex mixtures for keratinocyte-derived MVPs.

Results

To further confirm PAFR involvement in UVB-MVP release, we treated HaCaT keratinocytes with UVB or the metabolically stable PAFR agonist carbamoyl-PAF (CPAF), which resulted in increased MVP levels in cellular supernatants as soon as 2 hours after treatment (Figure 1A). Similar findings were noted in immortalized N/TERT and primary human keratinocytes (Supplemental Figure 1; supplemental material available online with this article; https://doi.org/10.1172/JCI144963DS1). The highest fluences of UVB used resulted in only approximately 20% cell death (Supplemental Figure 2). As signal transduction pathways that regulate MVP release, including p38 MAPK, ERK, NF-κB, are downstream of PAFR activation (16–18), we next tested pharmacologic inhibitors of these pathways for their abilities to modulate UVB- and CPAF-mediated MVP release in HaCaT keratinocytes. Inhibitors of the p38 MAPK, ERK, and NF-κB pathways all attenuated the stimulation

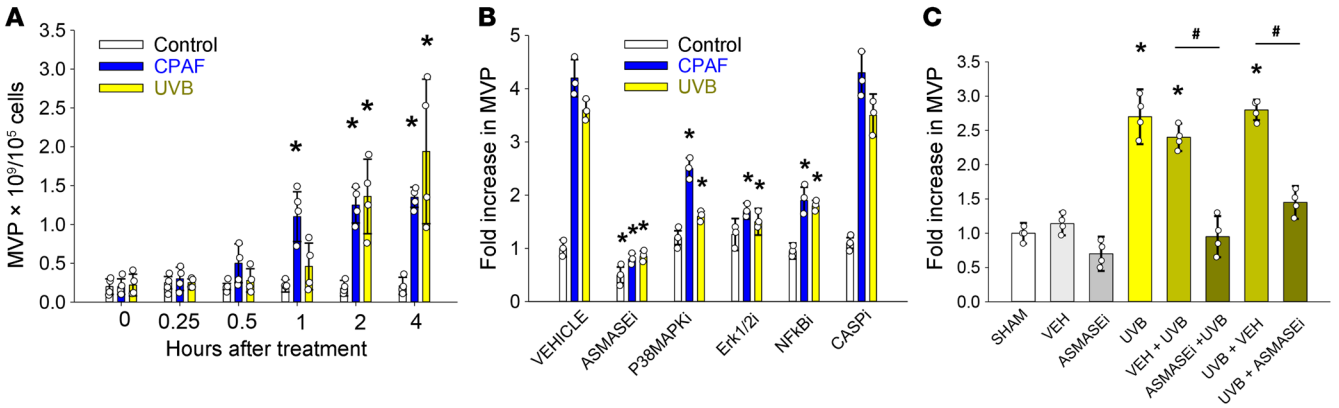

Figure 1. UVB-induced MVP release in HaCaT keratinocytes and human skin explant tissue. For the in vitro studies, (**A**) HaCaT keratinocytes were treated with 0.1% ethanol vehicle control, 100 nM CPAF, or 3600 J/m^2 UVB, and the levels of MVPs released into the supernatants were measured at various time points. (**B**) HaCaT keratinocytes were treated with CPAF or UVB and an inhibitor (i) of aSMase (imipramine, 50 μM), P38 MAPK (SB 203580, 10 μM), ERK 1/2 (PD 98,059, 10 μM), NF-κB (PDTC, 10 μM), or pan-caspase (Z-VAD-FMK, 24 μM) 1 hour before CPAF or UVB treatment or immediately after UVB (imipramine) treatment. The levels of MVPs released into the supernatants were measured 4 hours later. (**C**) For the ex vivo studies, human skin explants were either untreated or treated with vehicle (VEH) (90% ethanol plus 10% DMSO), the aSMase inhibitor imipramine (500 μM), UVB (2500 J/m^2), or imipramine or vehicle 30 minutes before or immediately following UVB irradiation. Four hours later, MVPs were quantified in skin biopsies. The data in **A**–**C** are presented as the mean ± SD of 3 (**B**) or 4 (**A** and **C**) independent experiments. $^{\#}P < 0.05$; $^{*}P < 0.05$ versus control (**A**), vehicle (**B**), or sham (**C**), by 1-way ANOVA.

of MVP release (Figure 1B), supporting the concept that PAFR signaling mediates UVB-MVP release. Yet the pan-caspase inhibitor Z-VAD-FMK exerted no effect on stimulated MVP release, suggesting that apoptosis may not be involved. Ex vivo studies demonstrated that UVB elicited similar MVP release responses in human skin explant tissue (Figure 1C). Dosage- and time-response studies in WT C57BL/6 mice further revealed that UVB induced MVP release in a dosage- and time-dependent manner, with the maximal numbers of skin UVB-MVPs released approximately 4–8 hours after UVB exposure (Figure 2, A and B).

Stimulus-mediated translocation of the enzyme acid sphingomyelinase (aSMase) from lysosomes to plasma membranes is a common lipid pathway mediating MVP release (19, 20). Interestingly, PAFR activation has been reported to induce membrane translocation of aSMase and increase its enzymatic activity (21, 22). Several lines of evidence link aSMase as the effector for PAFR-mediated MVP release. First, HaCaT keratinocytes responded to CPAF and UVB with increased aSMase enzymatic activity (Supplemental Figure 3). Second, treatment with the aSMase inhibitor imipramine (23) after UVB irradiation blocked stimulated MVP release in HaCaT cells (Figure 1B), human skin explants (Figure 1C), and murine skin (Figure 2C). Finally, use of PAFR-KO (*Ptafr*$^{-/-}$) and aSMase-KO (*Spmd1*$^{-/-}$) mice confirmed the roles of PAFR and aSMase in UVB-MVP release in skin tissue (Figure 2C). Topical application of the aSMase product C2 ceramide, but not biologically inactive dihydroceramide (24), resulted in increased MVPs in *Spmd1*$^{-/-}$ mice (Figure 2C). These studies indicate that UVB generates MVPs in a process involving PAFR signaling and aSMase.

An important knowledge gap in photobiology is how keratinocytes transmit UVB-generated signals systemically. To determine whether UVB-MVPs can potentially serve this role, we tested if keratinocyte-derived MVPs could be measured in plasma following UVB irradiation of skin. As shown in Figure 2, D and E, UVB irradiation of the back skin of WT mice resulted in increased levels of plasma MVPs. Kinetics of plasma UVB-MVPs closely resembled that of skin-derived UVB-MVPs (compare Figure 2, A and B, with Figure 2, D and E). To confirm the keratinocyte origin of the increased plasma MVPs, we tested the expression of the membrane protein CaSR, which has been demonstrated to be expressed in keratinocytes and other epithelial tissues (25). Immunocytochemical studies (Supplemental Figure 4) confirmed that HaCaT and epithelial PFAR-expressing KB (KBP) cells, but not fibroblasts, were CaSR positive. Flow cytometric analysis revealed that MVPs released from HaCaT and N/TERT cells were positive but that fibroblasts and endothelial cells were negative for the CaSR (Supplemental Figure 5). Ex vivo studies using vacuum-generated blisters on human skin explants treated with UVB or topical CPAF (11) generated increased numbers of CaSR-positive MVPs in blister fluid compared with the control (Supplemental Figure 6), suggesting that epidermal keratinocytes were a significant source of the increased MVPs in the blister fluid. These studies indicate that the CaSR can be used as a marker to track keratinocyte-derived MVPs. Murine plasma MVPs measured after UVB exposure expressed CaSR protein in a dose-dependent pattern similar to that observed with cutaneous MVP release (Supplemental Figure 7), consistent with the notion that some of these blood MVPs were derived from epidermal keratinocytes following UVB irradiation.

We next confirmed the UVB effects on systemic MVP release in humans. As shown in Figure 3A and Supplemental Table 1, pilot studies testing the effect of acute UVB irradiation on human skin in vivo demonstrated a 2-fold increase in MVPs in skin biopsies 4 hours after treatment following a clinically relevant (1000 J/m^2 UVB, which is approximately 2.5 times the minimal erythema dose for patients with Fitzpatrick types I and II phototypes) UVB fluence. To determine whether UVB irradiation of large surface areas of human skin results in systemic UVB-MVPs, we enrolled participants undergoing medical phototherapy with a narrow-band (311 nm) UVB source in our dermatology clinic. Blood plasma MVPs were quantified before and 2 and 4 hours after treatment. As

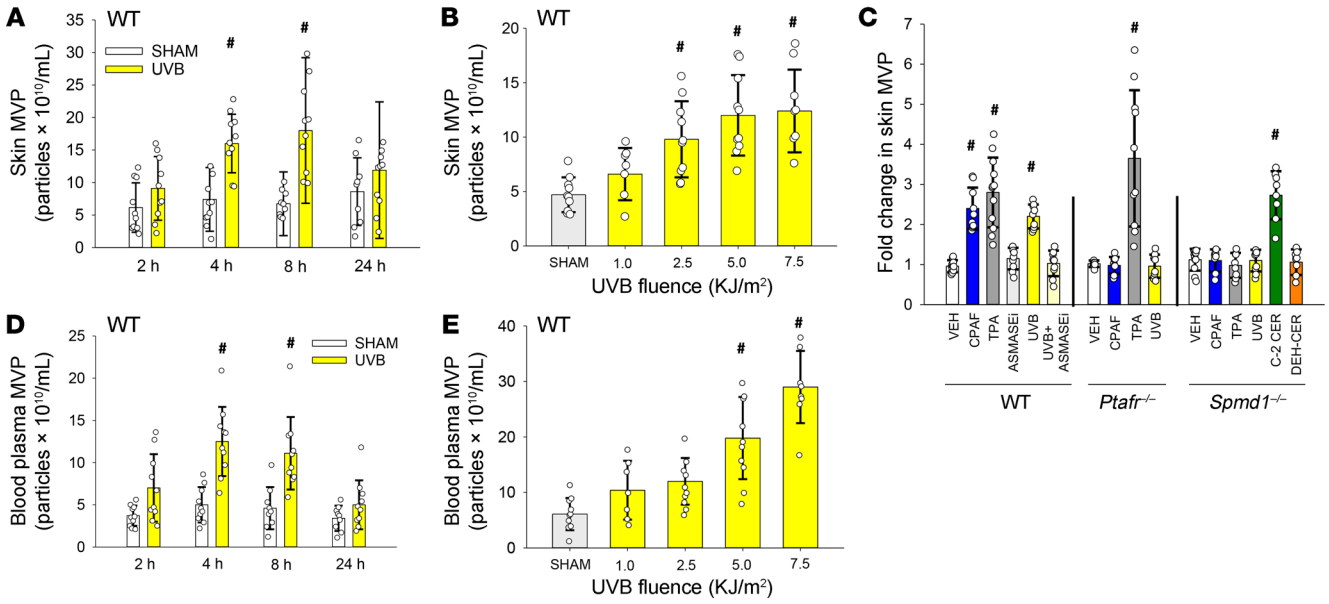

Figure 2. UVB-induced MVP release requires PAFR activation and aSMase. Groups of 7–10 WT mice were treated with sham or 7500 J/m² UVB for various durations, and MVPs were quantified in (**A**) skin tissue and (**D**) blood plasma. Groups of 8–10 WT mice were treated with various UVB fluences, and 4 hours later, MVPs were quantified in (**B**) skin tissue and (**E**) blood plasma. (**C**) Groups of 8–12 WT and PAFR- and aSMase-deficient mice were treated with sham, UVB (7500 J/m²), vehicle (90% ethanol plus 10% DMSO), CPAF (100 μM), TPA (100 μM), C2 ceramide (C2-CER) (20 μM), or inactive dihydroceramide (DEH-CER) (20 μM). Four hours later, duplicate skin biopsies were obtained and weighed, and MVPs were quantitated. Data are presented as the mean ± SD. #$P < 0.05$ versus sham (**A**, **B**, **D**, and **E**) or vehicle (**C**), by 1-way ANOVA.

depicted in Figure 3B and Supplemental Table 2, patients undergoing high-dose UVB treatments exhibited an almost 3-fold increase in MVP levels in plasma 4 hours after treatment. Flow cytometric analysis of plasma MVPs revealed that these subcellular bodies did not express appreciable levels of the CaSR at baseline, yet after UVB radiation, we detected a population of CaSR-positive MVPs (see Figure 3C). These studies using both preclinical and human models indicate that UVB-MVPs derived from keratinocytes can be found systemically.

Given that UVB irradiation stimulates the release of bioactive lipids and protein cytokines (6, 7), we tested MVPs derived from HaCaT keratinocytes treated with CPAF or UVB for the presence of 27 cytokines. As shown in Figure 4A for a group of representative cytokines and in Supplemental Table 3 for all the cytokines tested, most cytokine levels in UVB-MVPs were very low compared with levels in unstimulated MVPs. Of note, we found that levels of the IL-1 receptor antagonist, a cytokine with antiinflammatory properties (26), were elevated in UVB-MVPs.

UVB also generates PAF and oxidized glycerophosphocholine PAFR agonists (27). To assess whether PAFR agonistic lipids could also be found in keratinocyte-derived MVPs, we tested the PAFR biochemical agonistic activity of UVB-treated HaCaT keratinocytes. We measured PAFR agonist levels in the lipid extracts derived from cells versus those in supernatants at various time points after UVB treatment by exposing the lipid extracts to PAFR-positive KBP cells and measuring IL-8 release as a surrogate for PAFR activation, a validated biochemical assay that measures total PAFR activity (28–31). As shown in Figure 4B, five and ten minutes after UVB irradiation, the majority of PAFR agonistic activity (normalized to CPAF-induced IL-8 production in KBP cells) was cell associated. However, by 120 minutes after irradiation, the only appreciable PAFR agonistic activity was found in the supernatants. To confirm whether the supernatant-associated PAFR activity was due to MVPs, we separated MVPs from the supernatants and tested each sample. The majority of the PAFR agonistic activity resided in MVPs, not MVP-depleted supernatants (Figure 4C). We measured the PAFR agonistic activity in UVB-MVP lipid extracts at 120 minutes compared with various concentrations of a major PAF species (1-hexadecyl 2-acetyl-GPC), which revealed the equivalent of approximately 18 ng PAF in 5×10^{10} MVPs (Supplemental Figure 8). To confirm the PAFR biological activity of MVPs, we topically treated the dorsal ears of WT and PAFR-KO mice with lipid extracts from UVB-irradiated HaCaT MVPs, which resulted in increased ear thickness selectively in WT mice (Supplemental Figure 9). Finally, we removed MVPs from plasma of UVB-treated WT versus *Spmd1*$^{-/-}$ mice and found that only UVB-MVPs from WT mice showed PAFR activity (Supplemental Figure 10). These studies support the concept that UVB-MVPs contain functional PAF agonists and fit with our hypothesized model in Figure 4D showing that PAF agonists being generated in response to UVB residing in the cellular membranes activate the PAFR, which translocates aSMase, resulting in MVPs that then carry the PAF lipids. We propose that PAFR agonistic lipids are preserved in the MVPs, whereas acetylhydrolases remaining in the cell inactivate cell-associated PAF.

Given our findings that UVB-MVPs carry PAFR agonists and leave the epidermis, we next tested whether these novel effectors mediate the systemic immunosuppressive response ascribed to PAFR activation (3–7). To assess the UVB-MVP effects on immune competence, WT, *Ptafr*$^{-/-}$, and *Spmd1*$^{-/-}$ mice received

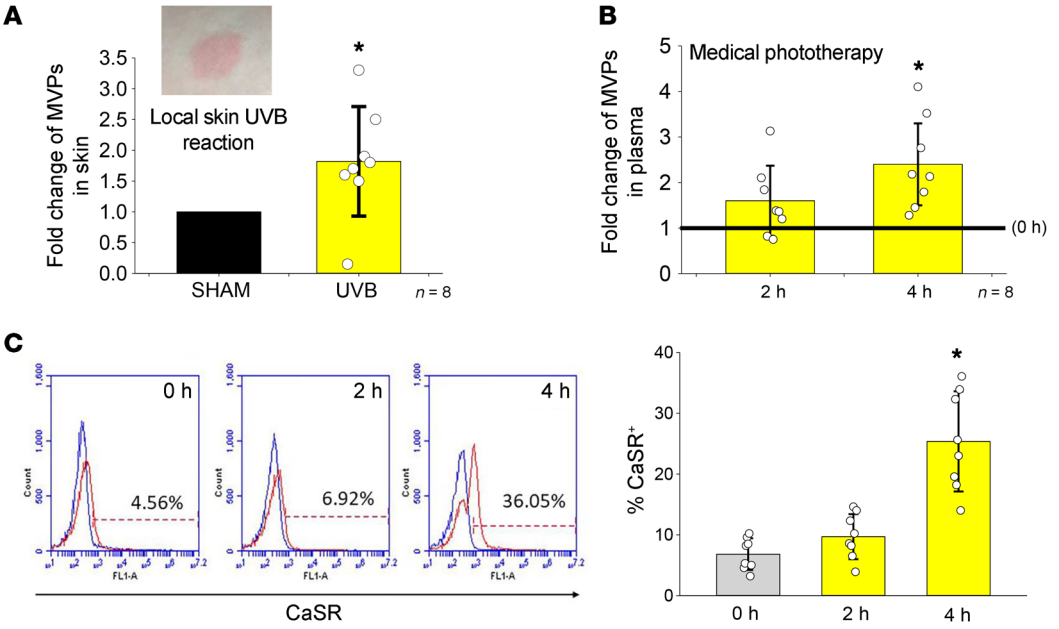

Figure 3. UVB-MVPs are released in human skin and blood plasma. (**A**) A group of 8 participants (see Supplemental Table 1) were exposed to 1000 J/m^2 UVB on the volar forearm. Four hours later, skin biopsies were collected from both the UVB-irradiated (see example of UVB skin reaction) and nonirradiated areas and then weighed, and MVPs were quantitated. (**B**) Blood samples were collected from 8 clinical patients receiving narrow-band UVB phototherapy (see Supplemental Table 2) either before (0 h) or 2 or 4 hours after therapy. MVPs were isolated from blood plasma and quantified. (**C**) CaSR expression on blood plasma MVPs (n = 8) was analyzed by flow cytometry. MVPs were stained with isotype control (blue line) or CaSR antibodies (red line). CaSR-stained MVPs were identified using flow cytometry by exclusion of the isotype control–stained MVPs. Graph shows quantification of flow cytometric CaSR expression on blood plasma MVPs. Data are presented as the mean ± SD. Statistically significant differences were determined by 2-sided Student's t test (**A**) or 1-way ANOVA (**B** and **C**). *P < 0.05 versus sham (**A**) or 0 hours (**B** and **C**).

an immunosuppressive dose of UVB (7500 J/m^2), an i.p. injection of CPAF, or control treatments and were then subjected to a well-established delayed-type hypersensitivity protocol (5, 30, 31). As expected, both UVB irradiation of skin and systemic exposure to CPAF resulted in immunosuppressive responses (as measured by inhibition of the ear thickness responses after elicitation with the neoantigen dinitrofluorobenzene [DNFB]) in WT mice. However, UVB did not generate immunosuppressive responses in *Ptafr*$^{-/-}$ or *Spmd1*$^{-/-}$ mice (Figure 5A and Supplemental Figure 11). The ability of i.p. injections of CPAF to attenuate the DNFB elicitation responses in the *Spmd1*$^{-/-}$ mice indicates that these mice retained their ability to respond to PAFR-mediated immunosuppressive effects. Inhibition of skin MVP release by topical treatment with the aSMase inhibitor imipramine on WT mouse skin showed inhibitory effects similar to those seen in *Spmd1*$^{-/-}$ mice (Figure 5B and Supplemental Figure 12), suggesting that skin-released MVPs were involved in the UVB-induced immunosuppression. Topical imipramine did not attenuate CPAF-induced immunosuppressive effects. Systemic immunosuppression from various pro-oxidative stressors such as UVB involves upregulation of the cytokines IL-10 and TGF-β, with decreased IL-12 and IFN-γ and increased Treg differentiation (4–7). Thus, to confirm the functional testing, we assayed these critical cytokines and Treg levels in lymph nodes following UVB treatment of *Foxp3*^{EGFP} mice (31). As shown in Figure 5C, UVB generated increased mRNA levels of IL-10, TGF-β, and the Treg-associated gene *Foxp3* as well as the marker EGFP in *Foxp3*^{EGFP} mice. UVB similarly downregulated the Th1 cytokines IL-12A and IFN-γ in draining lymph nodes. It should be noted that the expression of all of these genes was normalized by application of the topical aSMase inhibitor imipramine.

Discussion

The current report indicates that bioactive MVPs are released from keratinocytes within hours of exposure to biologically relevant UVB fluences. Discovery of the keratinocyte-selective MVP marker CaSR revealed that UVB-MVPs can be found in the bloodstream. The selectivity of the CaSR for the keratinocyte is modest, as other epithelial cell types (e.g., renal epithelial) also express this membrane protein (25). Yet in the present studies, the increased levels of plasma MVP CaSR expression following UVB exposure in mice (Supplemental Figure 7) and in humans (Figure 3C) undergoing UVB treatments of widespread areas of skin fit with the concept that these MVPs are keratinocyte derived. Of interest, MVPs derived from homogeneous cultures of keratinocytes did not result in 100% expression of the CaSR (see Supplemental Figure 5), which could result in an underestimation of keratinocyte-derived MVPs when assayed in biologic specimens. Hence, the CaSR does have some limitations as a marker for keratinocyte MVPs.

The present studies demonstrated that these subcellular particles carry both cytokines and bioactive lipid PAF. Of interest, one of the cytokines that appeared to be upregulated in UVB-MVPs was the IL-1 receptor antagonist, a cytokine with well-known anti-inflammatory characteristics (26). The role of this cytokine in UVB responses is at present unclear, although theoretically, it could be involved in the therapeutic effects of phototherapy. With our dis-

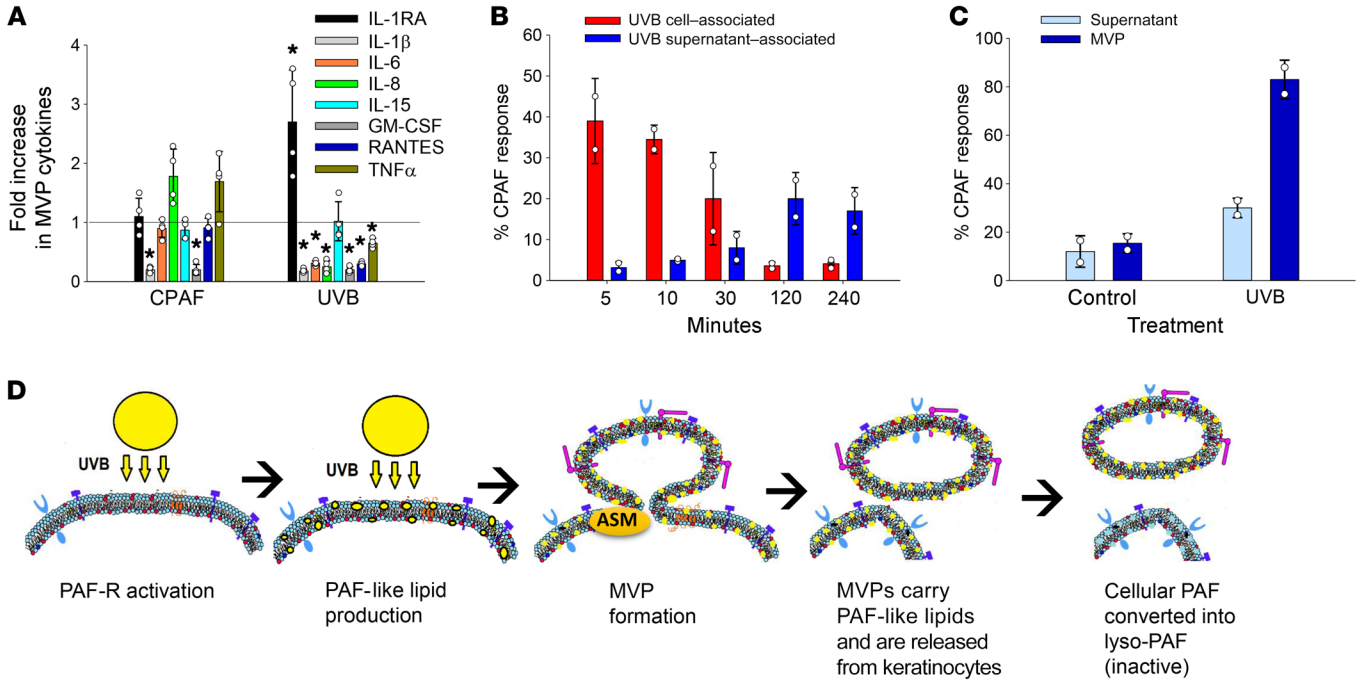

Figure 4. UVB-MVPs carry cytokines and PAF lipids. (**A**) HaCaT keratinocytes were treated with 100 nM CPAF or 3600 J/m^2 UVB. MVPs were isolated from cell supernatants 4 hours after treatment and analyzed for cytokine expression using the Bio-Plex Pro Human Cytokine 27-Plex Assay kit. Data are presented as the mean ± SEM of representative cytokines from 3 separate experiments (see Supplemental Table 3 for all cytokine values). *$P < 0.05$ versus control, by 1-way ANOVA. (**B**) Lipids extracted from UVB-treated HaCaT keratinocytes and culture medium were collected at various time points and tested for PAFR agonistic activity. PAFR-positive KBP cell release of IL-8 in supernatant was compared with 1 nM CPAF-induced IL-8 production in KBP cells. (**C**) HaCaT supernatants, 120 minutes after UVB treatment, were separated into MVP-positive and MVP-depleted supernatants, and lipids were extracted and then added to PAFR-positive KBP cells to test the PAFR agonistic response. Data in **B** and **C** are representative of duplicate samples from 3 separate experiments with similar results. (**D**) Hypothesized mechanism by which UVB generates PAFR agonists that activate the PAFR, resulting in aSMase activation and generation of MVP, which carry bioactive PAFR agonists, whereas cell-associated PAFR agonists are rapidly metabolized.

covery that UVB-MVPs have PAFR agonistic activity, the focus of the current studies was to define the role of PAF transported by these subcellular particles. Both the pharmacologic and genetic strategies aimed at the critical MVP-generating enzyme aSMase and the PAFR revealed that PAF carried in UVB-MVPs mediatef delayed systemic immunosuppression responses. Details from preclinical studies indicated that the relevant PAFR for this immunosuppressive response is on the mast cell (4–6). Hence, a logical interpretation of the present findings is that metabolically labile PAF travels from the epidermal keratinocyte to the mast cell via MVPs. As UVB-mediated systemic immunosuppression plays a role in diverse areas, from carcinogenesis to the treatment of proinflammatory disorders (4, 6, 7), we believe that the current mechanistic studies have clinical relevance. In summary, these studies offer insights into how keratinocytes transfer environmental signals systemically and provide potential therapeutic targets for addressing the adverse effects of UVB radiation exposure.

Methods

Chemicals/UVB. All chemicals were obtained from MilliporeSigma unless otherwise indicated. Phorbol ester 12-*O*-tetradecanoylphorbol-13 acetate (TPA) was used in cell lines, skin explants, and mice as a PAFR-independent stimulus, as TPA does not generate PAF in our model systems (28, 29, 31). For UVB treatment of cells, skin explants, mice, and human arms, we used a Philips F20T12/UVB lamp source with a Kodacel Filter (Kodak) to remove UVC (27, 28). The fluences used were based on previous studies by our group and others. In particular, for keratinocyte lines in vitro, fluences above 1.8 kJ/m^2 were needed to generate MVPs (10, 28). In addition, for human skin, fluences of 1.0 kJ/m^2 are needed to generate MVPs (11). This is an approximate fluence reported to generate immunosuppression on human skin (32). Finally, using mice on a C57BL/6 background, UVB fluences of at least 5 kJ/m^2 are needed to induce systemic immunosuppression (3, 5). Human phototherapy studies used a Daavlin nUVB UV 7 Series source.

Cell culture. Cell lines were grown as previously described (10, 17, 27). The HaCaT keratinocyte-derived cell line (provided by Petra Boukamp, German Cancer Research Center, Heidelberg, Germany) and the PAFR-positive KBP and control (PAFR-negative) KBM cells, generated as described previously (29), were grown in DMEM high-glucose media with 10% FCS. N/TERT and primary keratinocytes were grown in EpiLife medium with Human Keratinocyte Growth Supplement (Thermo Fisher Scientific). KBP/KBM cells were grown to 40% confluence, and HaCaT cells were grown to approximately 80%–90% confluence in 10 cm dishes. The cells were washed 3 times with HBSS and then incubated with HBSS plus 10 mg/mL fatty acid–free BSA for UVB exposures. Cells were either not treated or were treated with vehicle (0.1% ethanol), CPAF (100 nM), or imipramine (50 μM) before and after UVB irradiation (3600 J/m^2 UVB if not specifically mentioned). In some experiments, 100 nM TPA or 10 μM of the p38 MAPK inhibitor SB203580 (4-[4-(4-fluorophenyl)-2-(4-methylsulfin-

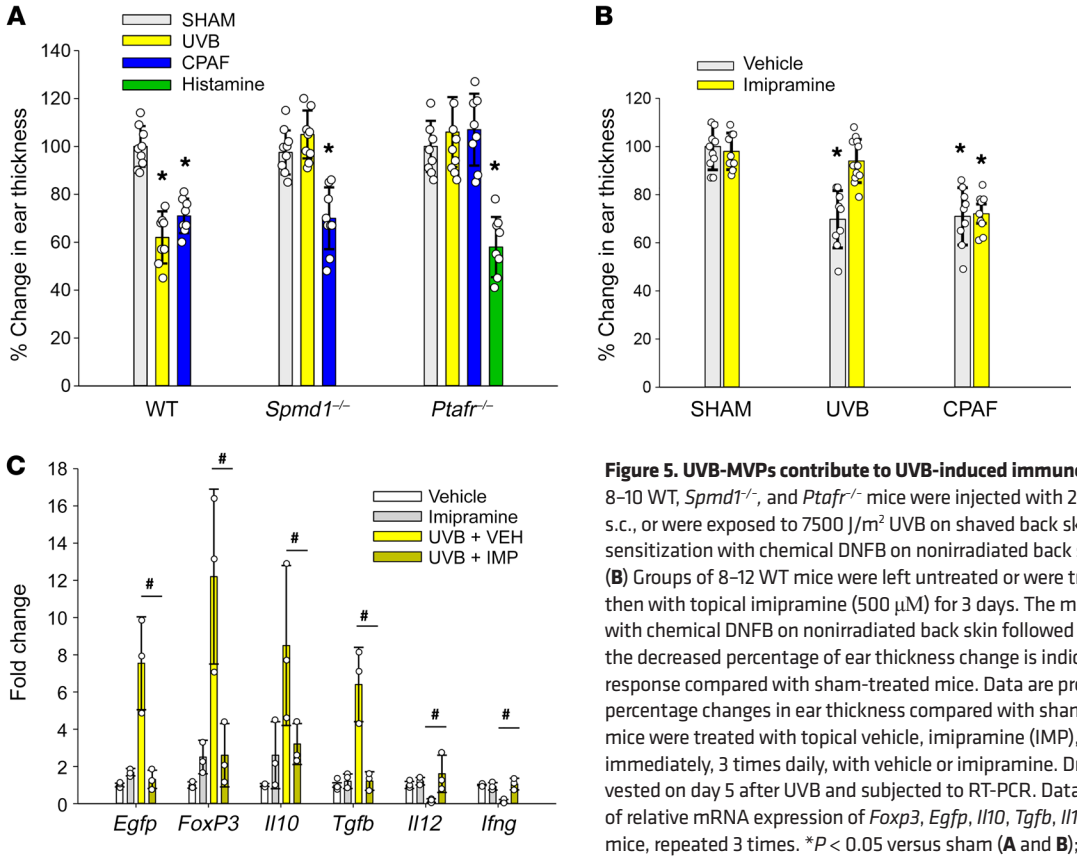

Figure 5. UVB-MVPs contribute to UVB-induced immunosuppression. (**A**) Groups of 8–10 WT, *Spmd1*$^{-/-}$, and *Ptafr*$^{-/-}$ mice were injected with 250 ng CPAF i.p. or 1 μg histamine s.c., or were exposed to 7500 J/m^2 UVB on shaved back skin. The mice then underwent sensitization with chemical DNFB on nonirradiated back skin followed by ear elicitation. (**B**) Groups of 8–12 WT mice were left untreated or were treated with UVB or CPAF and then with topical imipramine (500 μM) for 3 days. The mice then underwent sensitization with chemical DNFB on nonirradiated back skin followed by ear elicitation. For **A** and **B**, the decreased percentage of ear thickness change is indicated as a suppressed immune response compared with sham-treated mice. Data are presented as the mean ± SD percentage changes in ear thickness compared with sham values. (**C**) Groups of *FoxP3*^{EGFP} mice were treated with topical vehicle, imipramine (IMP), or 7500 J/m^2 UVB followed immediately, 3 times daily, with vehicle or imipramine. Draining lymph nodes were harvested on day 5 after UVB and subjected to RT-PCR. Data are presented as the mean ± SD of relative mRNA expression of *Foxp3*, *Egfp*, *Il10*, *Tgfb*, *Il12a*, and *Ifng* using groups of 3–4 mice, repeated 3 times. *$P < 0.05$ versus sham (**A** and **B**); #$P < 0.05$ (**C**), by 1-way ANOVA.

ylphenyl)-1H-imidazol-5-yl] pyridine), the ERK1/2 (MAPK/ERK kinase [MEK]) inhibitor PD98,059, the NF-κB inhibitor ammonium pyrrolidine dithiocarbamate (PDTC), or 24 μM of the pan-caspase inhibitor Z-VAD-FMK [carbobenzoxy-valyl-alanyl-aspartyl-(*O*-methyl)-fluoromethylketone] was given 1 hour before CPAF treatment (except for imipramine, which was given after UVB treatment). The MAPK and NF-κB inhibitor doses were the same as those used in our previous studies, as they have demonstrated select inhibition of the respective pathways (17, 28). The concentration of Z-VAD-FMK used was based on its ability to block UVB-mediated apoptosis in HaCaT cells (ref. 28 and data not shown). None of the chemicals used, except for imipramine, absorbed appreciably in the UVB spectrum.

Mice. Six- to 8-week-old female C57BL/6 WT mice (PAF-R–expressing) were purchased from Charles River Laboratories, and some male and female WT mice from our own colonies were also used. The PAFR-KO (*Ptafr*$^{-/-}$) mice on a C57BL/6 background were a gift from Takao Shimizu (University of Tokyo, Tokyo, Japan). The *Spmd1*$^{+/-}$ heterozygous mice, originally from Edward Schuchman's laboratory (19), were obtained from Irina Petrache's group at the National Jewish Medical Center (Denver, Colorado, USA). The aSMase KO (*Spmd1*$^{-/-}$) mice were bred with their heterozygous littermates. Eight- to 12-week-old Foxp3^{EGFP}-knockin transgenic mice on a C57BL/6 background were obtained from The Jackson Laboratory as previously reported (31). All mouse lines were rederived every 2 years. All mice were housed under specific pathogen–free conditions. Mice were i.p. injected with ketamine/xylazine (100 and 10 mg/kg, respectively), shaved, and were then either not treated or given vehicle (90% DMSO plus 10% ethanol), imipramine (500 μM), UVB (7500 J/m^2), and imipramine immediately after UVB treatment. After treatment for 4 hours, the mice were euthanized. Skin was collected by 6 mm punch biopsies. Tissues were cut up finely in the microcentrifuge tube and digested in 0.5 mL of 5 mg/mL collagenase and dispase solution overnight at 37°C for MVP isolation. Blood was collected from the heart in heparin-coated tubes and the blood plasma prepared immediately for MVP isolation.

Human skin explants. Deidentified discarded skin was obtained from human contouring (abdominoplasty and brachioplasty) surgeries (11, 28). Skin explants were washed, and the fat was trimmed, and then placed in PBS warmed at 37°C. Next, the explants were treated or not with 100 μL vehicle per 1 × 1 cm^2 area (90% DMSO plus 10% ethanol), or 500 μM imipramine, 2500 J/m^2 UVB, and imipramine 1 hour before UVB or immediately after UVB treatment. After 4 hours, skin was harvested by punch biopsies. Tissue samples were digested with collagenase/dispase solution overnight for MVP isolation (11, 28).

Human skin and blood preparation. For skin MVP collection, healthy donors were irradiated with 1000 J/m^2 UVB using the Philips F20T12/UVB lamp source on arm skin. After 4 hours, skin tissue were biopsied (5 mm punch biopsies) from irradiated and nonirradiated areas for MVP isolation. For blood plasma MVPs, patients who were on a stable dose of narrow-band UVB phototherapy (>20 treatments, with the last UVB treatment at least 4 days before the current treatment) were enrolled in this study. Before treatment and 2 and 4 hours after treatment, blood from participants undergoing phototherapy treatment of at least 80% of their body surface area (using a Daavlin nUVB source on the entire body except the groin area) was drawn into heparin-coated tubes and proceeded immediately for MVP isolation.

MVP isolation and analysis. MVPs were isolated from culture medium, skin biopsies, and blood plasma as previously reported (10, 11, 28). In brief, cell culture medium, skin biopsy lysates, and blood plasma were collected and centrifuged at 2000*g* for 20 minutes at 4°C to remove cells and debris. Skin biopsy tissue and blood plasma were then centrifuged at 20,000*g* for 10 minutes at 4°C to remove any remaining tissue and subcellular components. MVPs were then pelleted after 20,000*g* centrifugation of the sample supernatant for 70 minutes at 4°C. In some experiments exosomes were collected following an additional 170,000*g* centrifugation for 90 minutes. The concentrations of the MVPs and exosomes were determined using a NanoSight NS300 instrument (Malvern Panalytical). Three 30-second videos of each sample were recorded and analyzed with NTA software, version 3.0, to determine the concentration and size of the measured particles with the corresponding standard error. As shown in Supplemental Figure 13, MVPs were characterized by Western blotting as expressing annexin V with only low levels of the exosome-specific markers CD63 and TSG101. Moreover, transmission electron microscopy revealed MVPs with appropriate dimensions (Supplemental Figure 13).

Flow cytometry. MVPs were aliquoted into microcentrifuge tubes with similar concentrations. Each tube was stained with either 1 ng isotype control or 1 ng CaSR-FITC antibody (Novus Biologicals, catalog NB100-1830F). The samples were cultured in the dark at 4°C for 45 minutes. CaSR expression in MVPs was analyzed using a BD Accuri C6 Flow Cytometer (BD Biosciences). The percentage of CaSR-positive MVPs was derived by comparison of CaSR-stained MVPs with isotype control–stained MVPs.

Measurement of cytokines and chemokines. HaCaT keratinocytes were treated with vehicle (0.1% ethanol), CPAF (100 nM), or UVB (3600 J/m^2), and after 4 hours, the medium was collected for MVP isolation. MVPs were resuspended with 100 μL filtered PBS and stored at –80°C before the assay. Cytokine levels were measured with the Bio-Plex Pro Human Cytokine 27-Plex Assay kit (Bio-Rad) as previously reported (28). Cytokine concentration (pg/mL) was normalized to MVP numbers for analysis.

Measurement of PAFR agonistic activity. The presence and quantitation of PAFR agonists in lipid extracts derived from HaCaT keratinocytes and from MVPs isolated from murine plasma were assessed by the ability of lipid extracts to induce IL-8 release in PAFR-expressing, but not PAFR-deficient, KBM cells, as previously reported (28, 31). KB cells were originally derived from a patient with a nasopharyngeal carcinoma. These cells are a model for human keratinocytes yet lack PAFRs. The KB cells (obtained from American Type Culture Collection [ATCC]) were transduced with the MSCV2.1 retrovirus containing the PAFR (KBP). Control (KBM) cells were transduced with the empty MSCV2.1 retrovirus (29). Lipid extracts (33) were isolated either from UVB-treated HaCaT cells or total cell medium at various time points and HaCa-induced MVP or MVP-depleted supernatant at 2 hours. Lipids were added to PAFR-expressing KBP cells, and supernatants were removed at 4 hours. The ratio of IL-8 released by treated KBP cells was compared with 1 nM CPAF-treated KBP cells (positive control), which were used to determine the PAFR agonistic activity level. Some experiments tested these lipid extracts derived from MVPs on PAFR-negative KBM cells using TPA =as a positive control for IL-8 release (10, 28, 30).

Contact hypersensitivity studies. The contact hypersensitivity (CHS) study was performed according to the protocol previously published (5, 30, 31). Briefly, on day 0, WT, *Ptafr*$^{-/-}$, and *Spmd1*$^{-/-}$ mice either received no treatment or were given CPAF (250 ng i.p. injection), histamine (1 μg s.c. for *Ptafr*$^{-/-}$ mice), or UVB (7500 J/m^2) on a 2.5 × 2.5 cm shaved area of lower back skin (hair was removed using clippers 24 hours beforehand), with surrounding skin blocked off with heavy black paper. Five days later, nonirradiated upper back and shoulder skin (that had been previously shielded from UVB radiation using heavy opaque paper) was treated with 50 μL of 0.5% DNFB in 4:1 acetone/olive oil (v/v). Nine days after DNFB treatment, murine ear thickness was measured, and then 1 ear was treated with 10 μL of 0.5% DNFB and the other ear with vehicle alone. Murine ear thickness was measured again 24 hours later. The immunosuppressive effects were determined by the changes in ear thickness between DNFB- and vehicle-treated ears. Control animals that did not undergo the sensitization step revealed less than a 5% change in ear thickness following DNFB treatment. Histamine was used as a positive control in the PAFR-KO mice, as described in our previous report (5, 31).

Real-time PCR. Expression of cytokines and Tregs in skin draining lymph nodes from *Foxp3*^{EGFP} mice was analyzed by real-time PCR (RT-PCR) exactly as previously described (31). Total mRNA from murine skin draining lymph nodes was purified using the RNeasy Micro kit (Invitrogen, Thermo Fisher Scientific). cDNA was synthesized using iScript Supermix (Bio-Rad), and then RT-PCR analysis was performed using Advanced SYBR Green Supermix (Bio-Rad) according to the manufacturer's protocol. mRNA expression was normalized to *Actb* using the ΔCt method, and the amount of PCR product was calculated using the $2^{-\Delta\Delta Ct}$ method. See Supplemental Methods for the list of PCR primer sequences used.

Statistics. All statistical calculations were performed using GraphPad Prism, version 6.0 (GraphPad Software). Statistical significance was determined by 2-sided Student's *t* test or 1-way ANOVA with the Holm-Šídák post hoc test (α = 5%). A *P* value of less than 0.05 was considered significant.

Study approval. All studies involving mice were approved by the IACUC of Wright State University. All studies involving humans were approved by the IRB of Wright State University and followed Declaration of Helsinki Principles. Volunteers provided written informed consent before enrollment in the study.

Author contributions

LL, CAR, CK, EEC, DRC, RPS, JCB, YC, MGK, and JBT designed the studies. LL, AAA, KEF, PT, CB, BYW, CLM, BS, ZS, CAR, ARW, EEC, LEK, DRC, RPS, JW, CMR, MGK, and JBT performed experiments. LL, KEF, JCB, YC, DRC, CK, and JBT were involved in data analysis. BYW, ARW, CLM, BS, ZS, CAR, EEC, CK, RMJ, and JBT were involved in collecting human samples. JBT supervised the study. LL and JBT wrote the manuscript.

Acknowledgments

This research was supported in part by grants from the NIH (R01 HL062996, to JBT; ES031087, to JBT and YC; GM130583, to MGK; and R21 AR071110, to JCB) and a Veteran's Administration Merit Award (5I01BX000853, to JBT). The content is solely the responsibility of the authors and does not necessarily represent the official views of the NIH or the US Veterans Administration.

Address correspondence to: Jeffrey B. Travers, Wright State University Department of Pharmacology and Toxicology, Dayton Ohio, USA. Phone: 937.775.2463; Email: jeffrey.travers@wright.edu.

1. Liu-Smith F, et al. UV-induced molecular signaling differences in melanoma and non-melanoma skin cancer. *Adv Exp Med Biol*. 2017;996:27–40.
2. Madan V, et al. Non-melanoma skin cancer. *Lancet*. 2010;375(9715):673–685.
3. Walterscheid JP, et al. Platelet-activating factor, a molecular sensor for cellular damage, activates systemic immune suppression. *J Exp Med*. 2002;195(2):171–179.
4. Damiani E, Ullrich SE. Understanding the connection between platelet-activating factor, a UV-induced lipid mediator of inflammation, immune suppression and skin cancer. *Prog Lipid Res*. 2016;63:14–27.
5. Ocana JA, et al. Platelet-activating factor-induced reduction in contact hypersensitivity responses is mediated by mast cells via cyclooxygenase-2-dependent mechanisms. *J Immunol*. 2018;200(12):4004–4011.
6. Bernard JJ, et al. Photoimmunology: how ultraviolet radiation affects the immune system. *Nat Rev Immunol*. 2019;19(11):688–701.
7. Tse BCY, Byrne SN. Lipids in ultraviolet radiation-induced immune modulation. *Photochem Photobiol Sci*. 2020;19(7):870–878.
8. Tickner JA, et al. EV, microvesicles/microRNAs and stem cells in cancer. *Adv Exp Med Biol*. 2018;1056:123–135.
9. Lane RE, et al. Extracellular vesicles as circulating cancer biomarkers: opportunities and challenges. *Clin Transl Med*. 2018;7(1):14.
10. Bihl JC, et al. UVB generates microvesicle particle release in part due to platelet-activating factor signaling. *Photochem Photobiol*. 2016;92(3):503–506.
11. Fahy K, et al. UVB-generated microvesicle particles: a novel pathway by which a skin-specific stimulus could exert systemic effects. *Photochem Photobiol*. 2017;93(4):937–942.
12. Beyer C, Pisetsky DS. The role of microparticles in the pathogenesis of rheumatic diseases. *Nat Rev Rheumatol*. 2010;6(1):21–29.
13. Pelletier F, et al. Increased levels of circulating endothelial-derived microparticles and small-size platelet-derived microparticles in psoriasis. *J Invest Dermatol*. 2011;131(7):1573–1576.
14. Tu CL, et al. The extracellular calcium-sensing receptor is required for calcium-induced differentiation in human keratinocytes. *J Biol Chem*. 2001;276(44):41079–41085.
15. Owen JL, et al. The role of the calcium-sensing receptor in gastrointestinal inflammation. *Semin Cell Dev Biol*. 2016;49:44–51.
16. Zhang Y, et al. RGS16 attenuates galphaq-dependent p38 mitogen-activated protein kinase activation by platelet-activating factor. *J Biol Chem*. 1999;274(5):2851–2857.
17. Marques SA, et al. The platelet-activating factor receptor activates the extracellular signal-regulated kinase mitogen-activated protein kinase and induces proliferation of epidermal cells through an epidermal growth factor-receptor-dependent pathway. *J Pharmacol Exp Ther*. 2002;300(3):1026–1035.
18. Tran TV, et al. Blockade of platelet-activating factor receptor attenuates abnormal behaviors induced by phencyclidine in mice through down-regulation of NF-κB. *Brain Res Bull*. 2018;137:71–78.
19. Bianco F, et al. Acid sphingomyelinase activity triggers microparticle release from glial cells. *EMBO J*. 2009;28(8):1043–1054.
20. Record M, et al. Extracellular vesicles: lipids as key components of their biogenesis and functions. *J Lipid Res*. 2018;59(8):1316–1324.
21. Goggel R, et al. PAF-mediated pulmonary edema: a new role for acid sphingomyelinase and ceramide. *Nat Med*. 2004;10(2):155–160.
22. Lang PA, et al. Stimulation of erythrocyte ceramide formation by platelet-activating factor. *J Cell Sci*. 2005;118(pt 6):1233–1243.
23. Liangpunsakul S, et al. Imipramine blocks ethanol-induced ASMase activation, ceramide generation, and PP2A activation, and ameliorates hepatic steatosis in ethanol-fed mice. *Am J Physiol Gastrointest Liver Physiol*. 2012;302(5):G515–G523.
24. Goni FM, et al. Biophysical properties of sphingosine, ceramides and other simple sphingolipids. *Biochem Soc Trans*. 2014;42(5):1401–1408.
25. Leach K, et al. International union of basic and clinical pharmacology. CVIII. Calcium-sensing receptor nomenclature, pharmacology, and function. *Pharmacol Rev*. 2020;72(3):558–604.
26. Dinarello CA. The IL-1 family of cytokines and receptors in rheumatic diseases. *Nat Rev Rheumatol*. 2019;15(10):612–632.
27. Marathe GK, et al. Ultraviolet B radiation generates platelet-activating factor-like phospholipids underlying cutaneous damage. *J Biol Chem*. 2005;280(42):35448–35457.
28. Liu L, et al. Thermal burn injury generates bioactive microvesicles: evidence for a novel transport mechanism for the lipid mediator platelet-activating factor (PAF) that involves subcellular particles and the PAF receptor. *J Immunol*. 2020;205(1):193–201.
29. Pei Y, et al. Activation of the epidermal platelet-activating factor receptor results in cytokine and cyclooxygenase-2 biosynthesis. *J Immunol*. 1998;161(4):1954–1961.
30. Zhang Q, et al. Staphylococcal lipoteichoic acid inhibits delayed-type hypersensitivity reactions via the platelet-activating factor receptor. *J Clin Invest*. 2005;115(10):2855–2861.
31. Sahu RP, et al. Cigarette smoke exposure inhibits contact hypersensitivity via the generation of platelet-activating factor agonists. *J Immunol*. 2013;190(5):2447–2454.
32. Matthews YJ, et al. A UVB wavelength dependency for local suppression of recall immunity in humans demonstrates a peak at 300 nm. *J Invest Dermatol*. 2010;130(6):1680–1684.
33. Bligh EG, Dyer WJ. A rapid method of total lipid extraction and purification. *Can J Biochem Physiol*. 1959;37(8):911–917.